CRYSTAL GROWTH & DESIGN

pubs.acs.org/crystal

Communication

Variation of Spin-Transition Temperature in the Iron(III) Complex Induced by Different Compositions of the Crystallization Solvent

Published as part of a Crystal Growth and Design virtual special issue on Molecular Magnets and Switchable Magnetic Materials

Ivan Nemec,* Lucie Kotásková, and Radovan Herchel*

Cite This: *Cryst. Growth Des.* 2023, 23, 1323−1329

Read Online

ACCESS | Metrics & More | Article Recommendations | Supporting Information

ABSTRACT: We crystallized the Schiff-base iron(III) spin-crossover complex [Fe(3,5Cl-L5)(NCSe)] from different two-component solvent mixtures containing methanol and chloroform ($\Phi = V(CH_3OH)/V(\text{solvent}) = 0.05$, 0.25, 0.50, 0.83, and 1.00). The obtained crystalline products were characterized by X-ray diffraction, and it was confirmed that they are all composed of the same crystalline phase, and they do not contain any crystal solvent. However, significant differences in magnetic properties were observed, and thermal hysteresis changed from (in K) $121T_{\downarrow}$ and $134T_{\uparrow}$ for $\Phi = 0.05$ and 0.25, down to $72T_{\downarrow}$ and $96T_{\uparrow}$ for $\Phi = 1.00$. The crystal structures of the low-spin and high-spin phases were studied theoretically and experimentally.

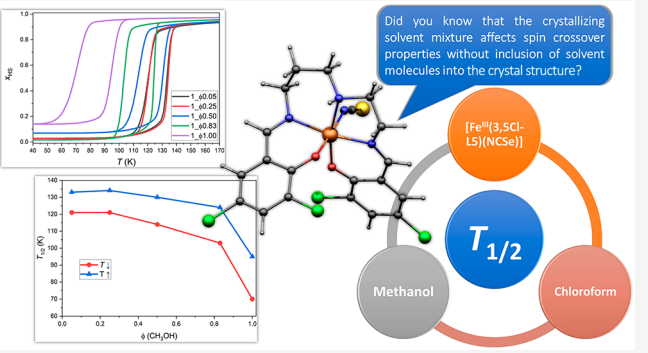

The tunability of the spin-crossover (SCO) behavior is an important assumption for versatile applications of SCO materials. Beneficially, SCO parameters such as thermal hysteresis width, transition temperature ($T_{1/2}$), cooperativity degree, curve abruptness, and completeness can be manipulated by sample modifications. The effect of the presence[1−3] and loss[4] of a solvent molecule in the lattice, the selection of an anion,[5,6] as well as the choice of a side substituent[6−8] are well-known strategies for modifying the SCO behavior. Also, metal dilution represents a sophisticated approach for modification of the SCO behavior and observing of the cooperativity degree and transition temperature of SCO materials. The SCO behavior can be also tuned by a postsynthetic modification as was manifested by solid state performed anion metathesis.[9]

Our ongoing interest in the magnetic behavior of Fe(III) complexes with pentadentate Schiff base ligands has brought remarkable results on distinct magnetic behaviors of polymorphs within this class of compounds,[10] or hydrogen bonding induced modification of $T_{1/2}$.[11] Recently, a new report on SCO with broad thermal hysteresis observed for an Fe(III) complex with a pentadentate Schiff base ligand $H_2$3,5Cl-L5 (*N*,*N*′-bis(1-hydroxy-3,5-dichloro-2-benzyliden)-1,6-diamino-4-azahexane) has been reported by Renz et al. which naturally caught our attention.[12] Complex [Fe(3,5-Cl-L5)(NCSe)] (**1**) exhibits thermally induced SCO with 24 K wide thermal hysteresis ($T_{1/2}$ = 99↓ and 129↑ K). From the comparison of the low-spin (LS, $S = 1/2$) and high-spin (HS, $S = 5/2$) crystal structures, it is apparent that reorganization of noncovalent interactions (H···Cl and Cl···Cl) happens upon spin transition. This, if significant, could explain the observation of the wide thermal hysteresis. In the original report,[12] the authors did not investigate this possibility in greater detail, and therefore, our original motivation for studying this system was to extensively theoretically and experimentally investigate the LS and HS crystal structures of **1**.

For the preparation of **1** we used a procedure similar to that in the original report,[12] but instead of an ultrasonic bath we used a standard magnetic stirrer. The reaction between [Fe(3,5-Cl-L5)Cl] and KNCSe in pure methanol led to precipitation of a brown microcrystalline powder, which was filtered off using a paper filter. For the preparation of the single-crystals suitable for X-ray diffraction experiments we used the remaining mother liquor which was crystallized isothermally. After several days thin needle-like crystals were obtained. First, we collected the diffraction data for the HS state (150 K), and then we attempted to measure the LS state crystal structure at 90 K as was done in the original report.[12] To our surprise, the measurement revealed the crystal structure with the very same metal−ligand bond lengths and unit cell parameters as was observed for the HS phase. Obviously, this

Received: December 1, 2022
Revised: February 14, 2023
Published: February 16, 2023

https://doi.org/10.1021/acs.cgd.2c01411
Cryst. Growth Des. 2023, 23, 1323−1329

did not match the previously reported magnetic properties.[12] Therefore, we measured the temperature dependence of the magnetic moment (μ_{eff}/μ_B) for two obtained fractions, needle-like crystals (**1_Φ1**) and microcrystalline powder precipitate (**1_Φ1p**). The measurements confirmed the presence of SCO with thermal hysteresis for both batches; however, the critical temperatures and profiles of magnetic functions were different (Figure 1). The **1_Φ1** batch exhibited much lower $T_{1/2}$ (72↓

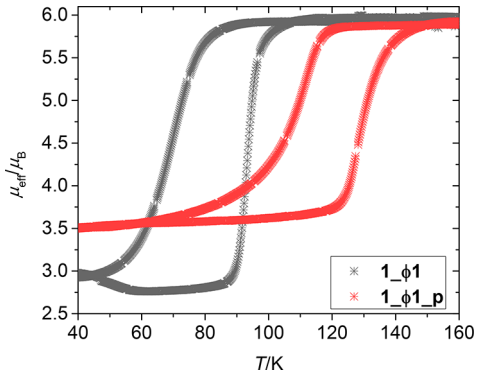

Figure 1. Temperature dependence of μ_{eff}/μ_B for **1_Φ1** and **1_Φ1p**.

and 96↑ K, ΔT = 24 K) than **1_Φ1_p** (106↓ and 129↑ K, ΔT = 23 K, Figure 1). Powder X-ray diffraction undoubtedly confirmed that both samples were the same crystallographic phase identical to the HS structure of **1** (Supporting Information, Figure S6–S7).

Inspired by this intriguing inconsistency, we investigated this phenomenon in greater detail. From magnetic measurements it is apparent that the low $T_{1/2}$ was observed for the batch composed of crystals which grew more than 5 days, whereas the high $T_{1/2}$ was observed for the precipitate. Therefore, one of the tested hypotheses was that different critical temperatures were related to the crystallinity of the samples, which is related to the time of the crystallization. In an attempt to prepare crystals, whose crystallization spans different time periods, we modified the composition of crystallization solutions from pure CH_3OH to solutions with a growing portion of $CHCl_3$. $CHCl_3$ was chosen as the second solvent because it dissolves **1** very well; it does not enter the crystal structure of **1** (does not form a solvate) and has a similar boiling temperature as CH_3OH. Therefore, it could be expected that the crystallization of **1** will be governed by slow evaporation of the solvent mixture. This mixture gradually loses slightly more $CHCl_3$ than CH_3OH molecules (because of higher vapor pressure of $CHCl_3$), and thus the solubility of **1** should be continuously decreasing. Four different crystallization mixtures with a different volume fraction Φ of CH_3OH were prepared (Φ = 0.83, 0.50, 0.25 and 0.05), and the corresponding crystalline samples (**1_Φ0.83**, **1_Φ0.50**, **1_Φ0.25**, **1_Φ0.05**) were obtained. In the case of the solutions with Φ > 0.5 also microcrystalline precipitates **1_Φ0.83p** (besides already prepared **1_Φ1_p**) were obtained and were included into this study. The purity of all the prepared samples was confirmed by X-ray powder diffraction. It must be noted that in the case of one of the precipitates (**1_Φ1_p**), the presence of KCl impurity was detected as this is a side product of the ligand metathesis (Cl^- ligand was substituted by KNCSe). We decided not to wash the precipitates with water (which would dissolve the impurity), because it would introduce a third solvent into the studied system. Furthermore, the presence of the diamagnetic KCl should not affect the SCO temperatures.

1 crystallizes as very thin needle-shaped crystals. The symmetry of the crystals is monoclinic with the $P2_1/n$ space group (see Supporting Information, Table S1). The crystal structures of LS and HS phases were well described in the original report,[12] and we will not add a new structural description here.

The best quality crystals were obtained for the batch **1_Φ0.25**. Again, we opted to measure the LS and HS crystal structures using a selected single crystal from this batch. We monitored SCO using diffraction methods. Therefore, we started the single crystal X-ray diffraction experiments at 140 K, and we collected sets of diffraction data at selected temperatures on cooling and also on heating. At 116 K (on cooling), a dramatic change in the quality of diffractions occurred as this was the $T_{1/2}$↓ temperature. The crystal structure of **1_Φ0.25@↓116K** shows metal–ligand (ML) bond lengths significantly shorter (Table S2) than observed at higher temperatures and in very good agreement with the LS structure of **1** reported in the original paper.[12] Upon further cooling (down to 108 K), neither the M–L bond lengths nor the unit cell parameters changed significantly, and therefore, we can conclude that the full HS → LS spin conversion occurred between 116 and 117 K (Figure 2). Upon heating, we

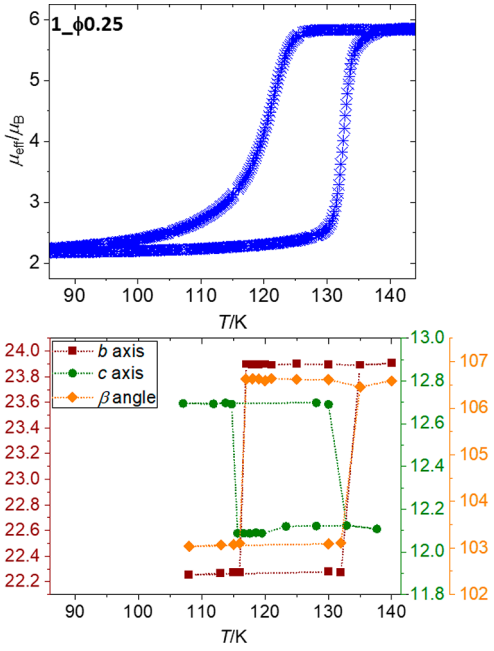

Figure 2. Temperature dependence of μ_{eff}/μ_B for **1_Φ0.25** (top) and the temperature dependence of the selected unit cell parameters as determined from the single crystal X-ray diffraction experiment for **1_Φ0.25** (bottom).

detected the LS → HS transition between 133 (LS) and 135 K (HS structure), whereas we were not able to get reasonable data from the measurement at 134 K. We attempted to also measure another SCO thermal cycle, but the crystal cracked upon another cooling. Here, we may conclude that the single crystal X-ray diffraction measurements confirmed that **1_Φ0.25** exhibits thermally induced SCO with hysteresis wide 18 K (if we assume $T_{1/2}$↑ to be 134 K). This is not in agreement with the magnetic data reported in the original

https://doi.org/10.1021/acs.cgd.2c01411
Cryst. Growth Des. 2023, 23, 1323–1329

paper,[12] but it is also not in good agreement with the magnetic data measured for **1_Φ1p**. Of note here is that the coordinates of the non-hydrogen atoms in the HS crystal structure of **1_Φ1** (at 90 K) are almost identical with those determined for **1_Φ0.25** (at 130 K, see Supporting Information, Figure S1) and thus, the difference in $T_{1/2}$ cannot be assigned to changes in the crystal structures.

We performed magnetic measurements for all the prepared batches. The results showed that all the samples show thermally induced spin crossover (Figure S2 and Figure S3). Remarkably, it is obvious that the batches prepared from the mixture with the largest content of methanol showed hysteretic loops shifted to lower temperatures, whereas the batches from the higher $CHCl_3$ content had hysteretic loops shifted to higher temperatures (Figure S2). The shift of hysteretic loops is observable also between **1_Φ0.83** and **1_Φ1**; however, the data for their precipitates **1_Φ0.83p** and **1_Φ1p** did not show a significant difference in $T_{1/2}$ (Figure S3). The hysteretic loops for the batches with the highest $CHCl_3$ content (**1_Φ0.25** and **1_Φ0.05**) are very similar, and they exhibit the highest $T_{1/2}$. The magnetic behavior of **1_Φ0.25** fits the temperature dependence of the unit cell parameters rather well (Figure 2). The observed behavior is reproducible.

The magnetic data were analyzed by using an Ising-like model (ISM) with Gaussian distribution of the cooperativity parameter derived by Boča et al.[13] Within the ISM defined by the Hamiltonian

$$\hat{H} = \frac{\Delta}{2}\hat{\sigma} - \Gamma\langle\sigma\rangle\hat{\sigma} \quad (1)$$

the transition between two spin states, $\sigma = -1$ for LS and $\sigma = +1$ for HS states, is governed by the energy difference between HS and LS states (Δ) and the cooperativeness of the system (Γ). Such a model can be modified to also include the distribution of the cooperativity parameter Γ in order to deal with the imperfections of the crystalline/powder samples by varying the standard deviation parameter σ of the Gaussian distribution function. The main advantage of such a model is its ability to reproduce the slope of the hysteresis loops, and hence better agreement with the experimental data can be achieved. Thus, the magnetic data were fitted by varying Δ, Γ, r_{eff}, and σ parameters within ISM, and subsequently calculated x'_{HS} for given temperature was used to calculate total molar susceptibility as

$$x''_{HS} = x'_{HS}(1 - x_{rHS}) \quad (2)$$

$$\chi_{mol} = (x''_{HS} + x_{rHS})\chi_{HS} + (1 - x''_{HS} - x_{rHS})\chi_{HS} \quad (3)$$

where x_{rHS} is the residual molar fraction of the HS state at a low temperature due to incomplete spin crossover, and x''_{HS} is rescaled high-spin fraction calculated from ISM resulting in the total high-spin mole fraction x_{HS} equal to $x_{HS} = x''_{HS} + x_{rHS}$. The molar susceptibility of the HS and LS species was calculated by the Curie law. The fitted parameters are listed in Table S3 and plotted in Figure 3 for crystal samples and in Figure S4 for microcrystalline precipitates. Evidently, there is small variation of the cooperativity Γ and entropy parameter r_{eff} within the prepared crystal batches of **1**, and variations of $T_{1/2}\downarrow$ and $T_{1/2}\uparrow$ are mainly due to a variation of Δ. Furthermore, there is a significant increase of the distribution parameter σ for the microcrystalline precipitates, Table S3.

We also theoretically attempted to investigate the impact of different solvents on the molecular geometry and the energies

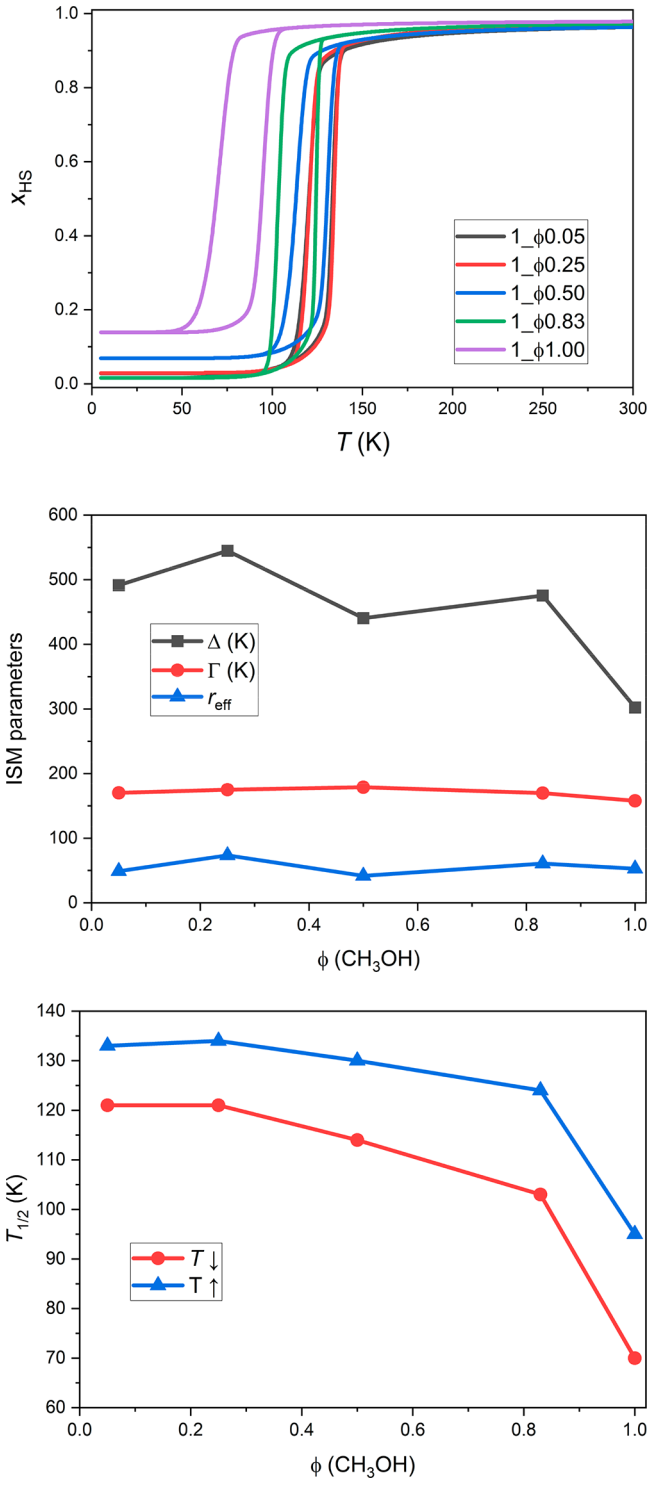

Figure 3. Temperature dependence the high-spin molar fraction x_{HS} according to ISM (top), the ISM parameters (middle), and transition temperatures (bottom) for crystalline samples of **1**.

of the LS and HS isomer of **1** using density functional theory (DFT) and utilizing ORCA 5.0 software.[14] We selected three functionals based on published benchmark studies,[15−17] namely, OPBE,[18] r^{2}SCAN,[19] and B3LYP* (B3LYP with reduced Hartree−Fock exchange to 15%)[20] and also included the atom-pairwise dispersion correction (D4).[21] The optimization was done in a vacuum, chloroform, and methanol with the C-PCM implicit solvation model.[22,23] Impact of

https://doi.org/10.1021/acs.cgd.2c01411
Cryst. Growth Des. 2023, 23, 1323−1329

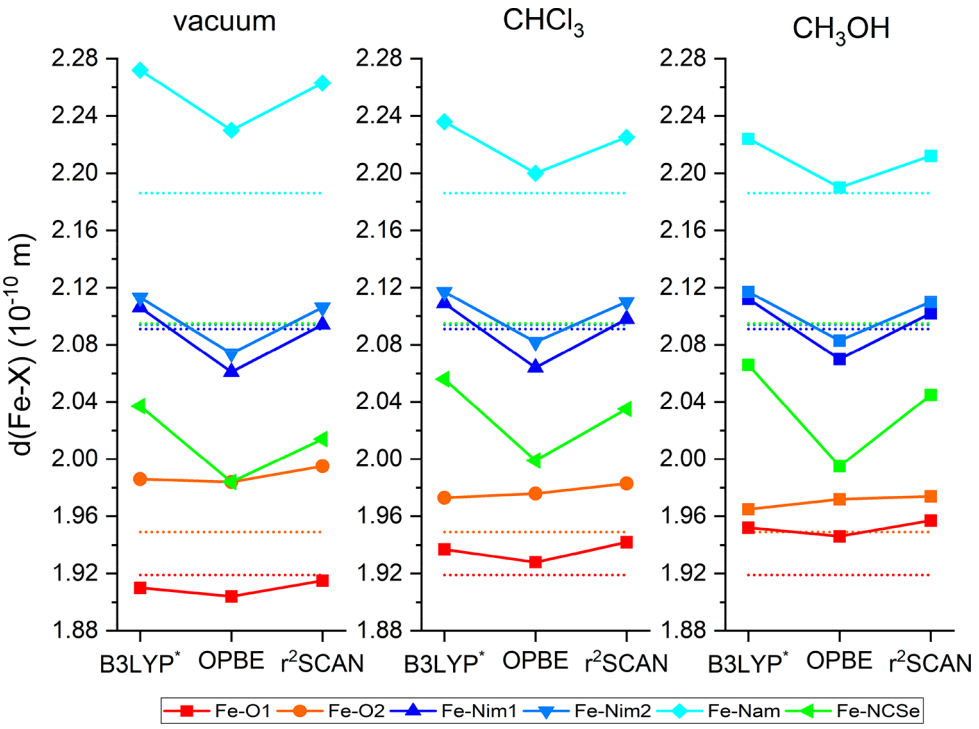

Figure 4. Graphical comparison of the donor−acceptor bond distances between X-ray data (dotted lines) and the respective DFT methods (B3LYP*, OPBE, and r^{2}SCAN) for the high-spin state of **1**.

solvents is demonstrated for the HS state of [Fe(3,5-Cl-L5)(NCSe)] in Figure 4. It seems that OPBE underestimates the Fe−NCSe bond, whereas B3LYP* and r^{2}SCAN overestimates the bond lengths to amino-nitrogen of 3,5-Cl-L5. In the case of the LS molecular geometries, OPBE heavily underestimates all Fe−N bond lengths (Figure S5). Moreover, there is also significant variation in bond lengths induced by the implicit solvation model, which points to the importance of intermolecular interactions.

The analysis of the electronic energy differences between the HS and LS isomers revealed positive values of $\Delta E_{el} = E_{el}^{HS} - E_{el}^{LS}$ for all three DFT functionals, and thus these functionals properly found the LS state with lower electronic energy (E_{el}), Table S4. As the molecular vibrations have a significant impact on the SCO properties, a better description is achieved with the energy difference corrected by the zero-temperature vibrational energy from the frequency calculation, ΔE_{el+ZPE}, which is depicted in Figure 5.

Apparently, ΔE_{el+ZPE} is significantly affected by applying the implicit solvation model, and both B3LYP*and r^{2}SCAN provided reasonable values of the HS-LS separation. Moreover, it seems that a more polar solvent like CH_3OH tends to increase ΔE_{el+ZPE}, and thus it stabilizes the LS state. This is in contradiction to the experimental finding (Figure 3 and Table S3), for which higher $\Phi(CH_3OH)$ yielded lower Δ and $T_{1/2}$ values. We can speculate that this discrepancy is caused by the implicit solvation approach which cannot grasp the effect of all intermolecular interactions properly, or the properties of **1** in the solid state simply cannot be encompassed by such an approach at all.

However, if the presented theoretical calculations are not deceptive, perhaps it most likely leads to the conclusion that the reported phenomenon is not governed by thermodynamics, but by the kinetics of the crystal growth of **1** under various contents of chloroform and methanol in crystallizing

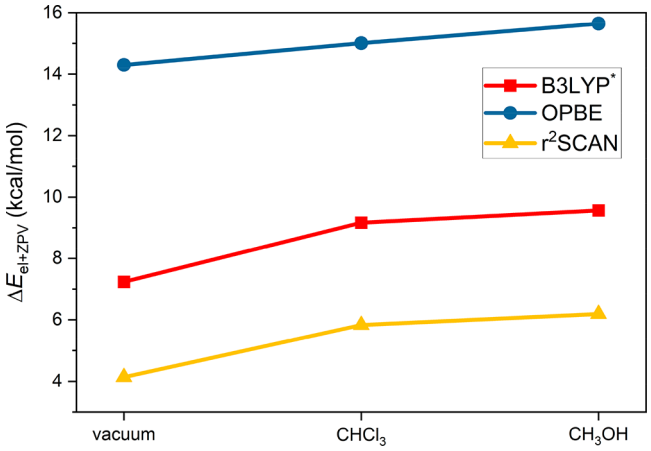

Figure 5. Graphical comparison the energy difference corrected by the zero-temperature vibrational energy from the frequency calculation ΔE_{el+ZPE} between the HS and LS states for different DFT methods applied to **1**.

solutions. Hence, the quality of the crystalline material and SCO properties are affected by a solvent mixture, but the solvent molecules do not cocrystallize. One of the possible approaches to test this hypothesis is to correlate parameters such as crystal mosaicity with the observed magnetic behavior. Therefore, we decided to prepare several batches of **1** crystallized at different crystallization rates. As was mentioned above, the best crystals were obtained in the batch of **1_Φ0.25**. However, the batches crystallized from solutions with a major chloroform fraction (**Φ0.25** and **Φ0.05**) have practically the same magnetic properties (Figure 3). Thus, we decided to crystallize **1** from **Φ0.5** and **Φ0.83** solutions, because **1_Φ0.5** and **1_Φ0.83** differ in $T_{1/2}\downarrow$ (114 K for **1_Φ0.5** and 103 K for **1_Φ0.83**), and their spin transition on

https://doi.org/10.1021/acs.cgd.2c01411
Cryst. Growth Des. 2023, 23, 1323−1329

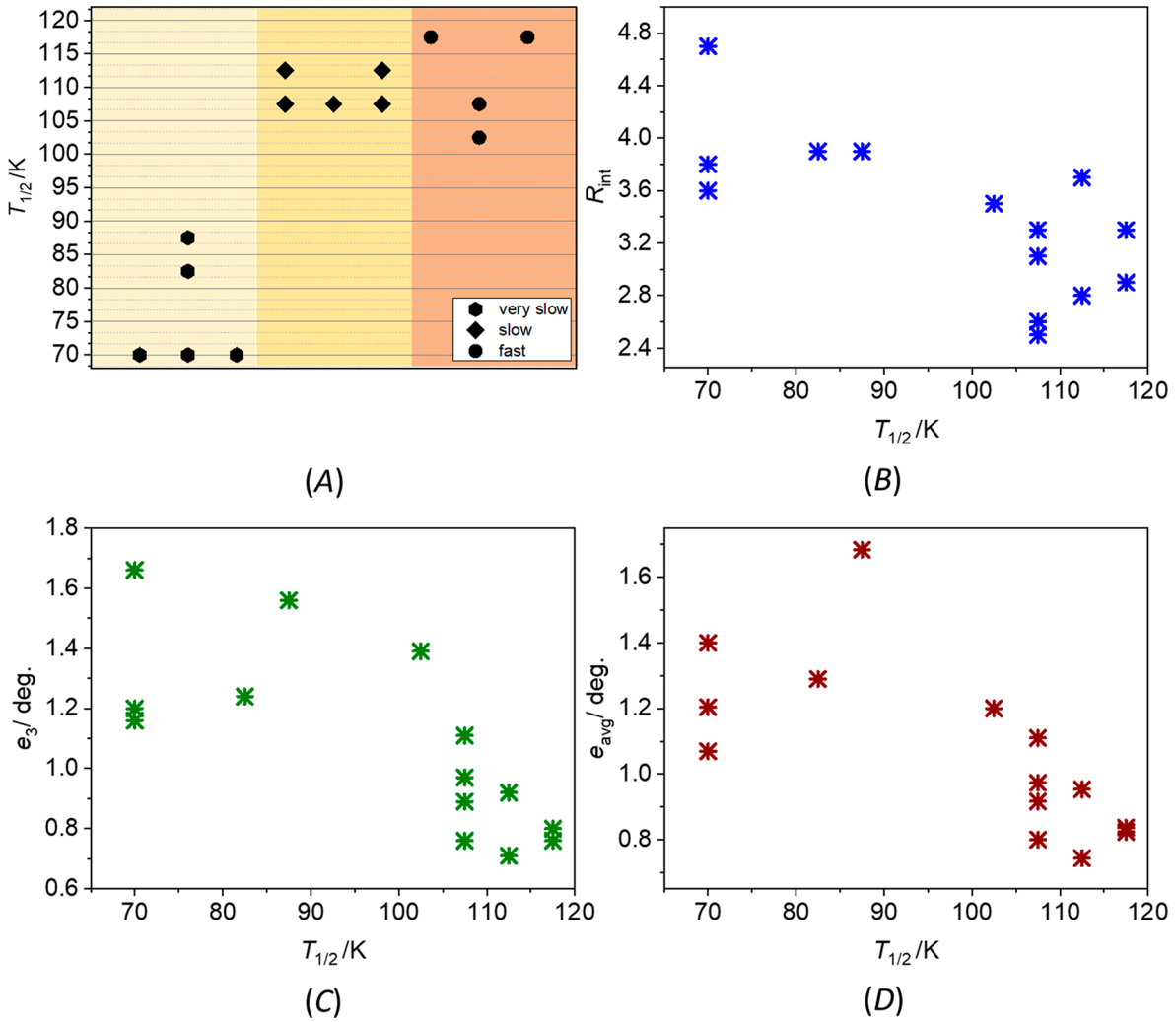

Figure 6. Plot of $T_{1/2}\downarrow$ versus crystallization rate (A). The colored boxes are used to highlight the crystallization rate, with a lighter color indicating slower crystallization. The plots of R_{int} vs $T_{1/2}\downarrow$ (B), e_3 vs $T_{1/2}\downarrow$ (C), and e_{avg} vs $T_{1/2}\downarrow$ (D). The value of e_{avg} was calculated as the arithmetic average of components e_1, e_2, and e_3. In all plots, the $T_{1/2}\downarrow$ value of crystals that remained in the high spin phase down to 80 K was assigned as 70 K for visualization purposes.

cooling is still accessible using standard commercial cryogenic devices (above 80 K). For preparation of the batches, we used the same reaction procedures as are described in Supporting Information, but the mother liquors were crystallized using three different crystallization rates: fast (≈1day), slow (up to 4 days), and very slow (≥7 days). The majority of the used single crystals were obtained for all the batches crystallized from **Φ0.5** solutions regardless of the rate of crystallization used. However, also very slow crystallization from the **Φ0.83** solutions resulted in the production of a few suitable single crystals.

The crystal mosaicity was determined taking into consideration the results of previous work on mosaicity in SCO complexes.[24] We set experimental conditions to be as identical as possible for all the investigated specimens. The experiment was conducted at 150 K, which is well above the highest $T_{1/2}\downarrow$ (Table S3). The data were collected using ω-scans (width 0.5 deg), and the exposition time was adjusted for each crystal based on its size, aiming for 0.83 Å resolution, completeness above 99%, data redundancy > 3, and $I/\sigma > 10$. As was already mentioned, the crystals of **1** are very thin (typically ≈0.05 mm in two dimensions), needle-like shaped growing in clumps of overlapping specimens, which makes it challenging to investigate the statistically relevant number of crystallites within a reasonable measurement time. Thus, we were capable of performing measurements for a limited number (14) of single crystals. It is important to note that the vast majority of the prepared crystals were not suitable for single-crystal experiments, and thus the results obtained only represent those crystals that met the necessary criteria.

After collecting each set of data at 150 K, we determined $T_{1/2}\downarrow$ for each crystal by measuring unit cell parameters starting from 125 K down to 80 K in decrements of 5 K. The occurrence of the SCO phenomenon was recorded between two measured temperature points, and the average of these values was used for visualization purposes. The $T_{1/2}\downarrow$ value of crystals that remained in the high spin phase at 80 K was set to 70 K for visualization purposes. The distribution of the determined $T_{1/2}\downarrow$ values is shown (Figure 6A). The results supported our hypothesis that the speed of crystallization affects the quality of crystals and the $T_{1/2}\downarrow$ value. Crystals crystallized in the "fast" and "slow" modes showed $T_{1/2}\downarrow$ values above 100 K. Crystals that crystallized "very slowly" showed

https://doi.org/10.1021/acs.cgd.2c01411
Cryst. Growth Des. 2023, 23, 1323−1329

$T_{1/2}\downarrow$ values below 90 K with most of them having $T_{1/2}\downarrow$ even below 80 K.

The results of the X-ray diffraction measurements were evaluated in the CrysAlisPro software.[25] As a first indication of the crystal quality, we inspected the equivalency of symmetry equivalent reflections (R_{int}) in the studied crystals. There is no strong correlation between $T_{1/2}\downarrow$ and R_{int}, but apparently, the crystals with lower $T_{1/2}\downarrow$ values tend to have larger R_{int} and *vice versa* (Figure 6B).

The CrysAlisPro software provides the mosaicity in three directions (e_1, e_2, and e_3) by fitting a Gaussian function to the peak.[26,27] Although these parameters do not measure the mosaicity directly, variations in the values of e_1, e_2, and e_3 can indicate changes in the mosaicity of the studied crystals and thus their quality.[28] Some authors only use the e_3 parameter due to its correlation with mosaicity values obtained from other data integration methods.[26] The results revealed that the e_2 component varied slightly among the measurements (0.76−0.96°), while larger variations were observed for e_1 (0.75−2.61°) and e_3 (0.71−1.66°). As per previous reports, for evaluation of mosaicity, we considered the values of e_3 and the arithmetic average (e_{avg})[29] of all three components e_1, e_2, and e_3 (Figure 6C−D, Table S5). As with R_{int}, the results for e_{avg} and e_3 did not show a strong linear correlation; however, crystals with higher $T_{1/2}\downarrow$ values tend to have lower values of e and e_3 and *vice versa*.

In summary, to the best of our knowledge, such an unprecedented solvent-induced variation of SCO spin-transition temperature as was discussed for **1** has not been reported yet. We showed that the different crystallization rates produced crystals exhibiting different SCO critical temperatures. Very slow crystallization (≥7 days) of the **Φ0.5** and **Φ0.83** solutions resulted into crystals exhibiting low SCO critical temperatures ($T_{1/2}\downarrow$ < 90 K), while faster crystallization (shorter than 4 days) led to larger $T_{1/2}\downarrow$ values (>100 K). The performed diffraction experiments indicate that crystals with low $T_{1/2}\downarrow$ values tend to have larger mosaicity parameters and R_{int}, and thus they are of lower quality than those with larger $T_{1/2}\downarrow$ values.

■ ASSOCIATED CONTENT

Supporting Information

The Supporting Information is available free of charge at https://pubs.acs.org/doi/10.1021/acs.cgd.2c01411.

Synthesis, crystallographic data, magnetic measurements, DFT calculation details, and powder diffraction patterns (PDF)

Accession Codes

CCDC 1909057 and 2223462−2223463 contain the supplementary crystallographic data for this paper. These data can be obtained free of charge via www.ccdc.cam.ac.uk/data_request/cif, or by emailing data_request@ccdc.cam.ac.uk, or by contacting The Cambridge Crystallographic Data Centre, 12 Union Road, Cambridge CB2 1EZ, UK; fax: +44 1223 336033.

■ AUTHOR INFORMATION

Corresponding Authors

Ivan Nemec − *Central European Institute of Technology, Brno University of Technology, 61200 Brno, Czech Republic; Department of Inorganic Chemistry, Palacký University, 77900 Olomouc, Czech Republic;* orcid.org/0000-0003-3231-7849; Email: ivan.nemec@upol.cz

Radovan Herchel − *Department of Inorganic Chemistry, Palacký University, 77900 Olomouc, Czech Republic;* orcid.org/0000-0001-8262-4666; Email: radovan.herchel@upol.cz

Author

Lucie Kotásková − *Central European Institute of Technology, Brno University of Technology, 61200 Brno, Czech Republic;* orcid.org/0000-0003-4825-3616

Complete contact information is available at: https://pubs.acs.org/10.1021/acs.cgd.2c01411

Author Contributions

The manuscript was written through contributions of all authors. All authors have given approval to the final version of the manuscript.

Notes

The authors declare no competing financial interest.

■ ACKNOWLEDGMENTS

The authors (I.N. and R.H.) acknowledge financial support from institutional sources of the Department of Inorganic Chemistry and Palacký University Olomouc, Czech Republic. We also acknowledge the CzechNanoLab Research Infrastructure supported by MEYS CR (LM2018110) for the measurement of some of the magnetic data. I.N. is grateful to Jakub Wojciechowski for discussions about mosaicity evaluation in CrysAlisPro software.

■ REFERENCES

(1) Bari, R. A.; Sivardière, J. Low-Spin-High-Spin Transitions in Transition-Metal-Ion Compounds. *Phys. Rev. B* **1972**, *5* (11), 4466−4471.

(2) Wajnflasz, J. Etude de La Transition "Low Spin"-"High Spin" Dans Les Complexes Octaédriques d'ion de Transition. *Phys. status solidi* **1970**, *40* (2), 537−545.

(3) Boča, R.; Linert, W. Is There a Need for New Models of the Spin Crossover? In *Molecular Magnets Recent Highlights*; Springer Vienna: Vienna, 2002; pp 83−100.

(4) Shakirova, O. G.; Lavrenova, L. G.; Kurat'eva, N. V.; Naumov, D. Y.; Daletskii, V. A.; Sheludyakova, L. A.; Logvinenko, V. A.; Vasilevskii, S. F. Spin Crossover in Iron(II) Complexes with Tris(Pyrazol-1-Yl)Methane. *Russ. J. Coord. Chem.* **2010**, *36* (4), 275−283.

(5) Halcrow, M. A. Structure:Function Relationships in Molecular Spin-Crossover Complexes. *Chem. Soc. Rev.* **2011**, *40* (7), 4119.

(6) Roubeau, O. Triazole-Based One-Dimensional Spin-Crossover Coordination Polymers. *Chem. - A Eur. J.* **2012**, *18* (48), 15230−15244.

(7) Arcis-Castíllo, Z.; Zheng, S.; Siegler, M. A.; Roubeau, O.; Bedoui, S.; Bonnet, S. Tuning the Transition Temperature and Cooperativity of Bapbpy-Based Mononuclear Spin-Crossover Compounds: Interplay between Molecular and Crystal Engineering. *Chem. - A Eur. J.* **2011**, *17* (52), 14826−14836.

(8) Feltham, H. L. C.; Johnson, C.; Elliott, A. B. S.; Gordon, K. C.; Albrecht, M.; Brooker, S. "Tail" Tuning of Iron(II) Spin Crossover Temperature by 100 K. *Inorg. Chem.* **2015**, *54* (6), 2902−2909.

(9) Askew, J. H.; Shepherd, H. J. Post-Synthetic Anion Exchange in Iron(II) 1,2,4-Triazole Based Spin Crossover Materials *via* Mechanochemistry. *Dalt. Trans.* **2020**, *49* (9), 2966−2971.

(10) Krüger, C.; Augustín, P.; Dlháň, L.; Pavlik, J.; Moncol', J.; Nemec, I.; Boča, R.; Renz, F. Iron(III) Complexes with Pentadentate Schiff-Base Ligands: Influence of Crystal Packing Change and Pseudohalido Coligand Variations on Spin Crossover. *Polyhedron* **2015**, *87*, 194−201.

(11) Nemec, I.; Herchel, R.; Trávníček, Z. The Relationship between the Strength of Hydrogen Bonding and Spin Crossover Behaviour in a Series of Iron(III) Schiff Base Complexes. *Dalt. Trans.* **2015**, *44* (10), 4474−4484.
(12) Rajnak, C.; Mičová, R.; Moncol, J.; Dlháň, L.; Krüger, C.; Renz, F.; Boča, R. Spin-Crossover in an Iron(III) Complex Showing a Broad Thermal Hysteresis. *Dalton Trans.* **2021**, *50* (2), 472−475.
(13) Boča, R.; Boča, M.; Dlháň, L.; Falk, K.; Fuess, H.; Haase, W.; Jaroščiak, R.; Papánková, B.; Renz, F.; Vrbová, M.; Werner, R. Strong Cooperativeness in the Mononuclear Iron(II) Derivative Exhibiting an Abrupt Spin Transition above 400 K. *Inorg. Chem.* **2001**, *40* (13), 3025−3033.
(14) Neese, F. Software Update: The ORCA Program System - Version 5.0. *WIREs Comput. Mol. Sci.* **2022**, *12*, e1606.
(15) Cirera, J.; Ruiz, E. Assessment of the SCAN Functional for Spin-State Energies in Spin-Crossover Systems. *J. Phys. Chem. A* **2020**, *124* (24), 5053−5058.
(16) Cirera, J.; Via-Nadal, M.; Ruiz, E. Benchmarking Density Functional Methods for Calculation of State Energies of First Row Spin-Crossover Molecules. *Inorg. Chem.* **2018**, *57* (22), 14097−14105.
(17) Siig, O. S.; Kepp, K. P. Iron(II) and Iron(III) Spin Crossover: Toward an Optimal Density Functional. *J. Phys. Chem. A* **2018**, *122* (16), 4208−4217.
(18) Perdew, J. P.; Burke, K.; Ernzerhof, M. Generalized Gradient Approximation Made Simple. *Phys. Rev. Lett.* **1996**, *77* (18), 3865−3868.
(19) Furness, J. W.; Kaplan, A. D.; Ning, J.; Perdew, J. P.; Sun, J. Accurate and Numerically Efficient r 2 SCAN Meta-Generalized Gradient Approximation. *J. Phys. Chem. Lett.* **2020**, *11* (19), 8208−8215.
(20) Reiher, M. Theoretical Study of the Fe(Phen)2(NCS)2 Spin-Crossover Complex with Reparametrized Density Functionals. *Inorg. Chem.* **2002**, *41* (25), 6928−6935.
(21) Caldeweyher, E.; Ehlert, S.; Hansen, A.; Neugebauer, H.; Spicher, S.; Bannwarth, C.; Grimme, S. A Generally Applicable Atomic-Charge Dependent London Dispersion Correction. *J. Chem. Phys.* **2019**, *150* (15), 154122.
(22) Garcia-Ratés, M.; Neese, F. Effect of the Solute Cavity on the Solvation Energy and Its Derivatives within the Framework of the Gaussian Charge Scheme. *J. Comput. Chem.* **2020**, *41* (9), 922−939.
(23) Barone, V.; Cossi, M. Quantum Calculation of Molecular Energies and Energy Gradients in Solution by a Conductor Solvent Model. *J. Phys. Chem. A* **1998**, *102* (11), 1995−2001.
(24) Lakhloufi, S.; Tailleur, E.; Guo, W.; Le Gac, F.; Marchivie, M.; Lemée-Cailleau, M.-H.; Chastanet, G.; Guionneau, P. Mosaicity of Spin-Crossover Crystals. *Crystals* **2018**, *8* (9), 363.
(25) *CrysAlisPro*, 1.171.42.49; Rigaku Oxford Diffraction, 2020.
(26) Harrison, K.; Wu, Z.; Juers, D. H. A Comparison of Gas Stream Cooling and Plunge Cooling of Macromolecular Crystals. *J. Appl. Crystallogr.* **2019**, *52* (5), 1222−1232.
(27) Kabsch, W. Integration, Scaling, Space-Group Assignment and Post-Refinement. *Acta Crystallogr. Sect. D Biol. Crystallogr.* **2010**, *66* (2), 133−144.
(28) Madsen, S. R.; Overgaard, J.; Stalke, D.; Iversen, B. B. High-Pressure Single Crystal X-Ray Diffraction Study of the Linear Metal Chain Compound Co3(Dpa)4Br2·CH2Cl2. *Dalt. Trans.* **2015**, *44* (19), 9038−9043.
(29) Farley, C.; Burks, G.; Siegert, T.; Juers, D. H. Improved Reproducibility of Unit-Cell Parameters in Macromolecular Cryocrystallography by Limiting Dehydration during Crystal Mounting. *Acta Crystallogr. Sect. D Biol. Crystallogr.* **2014**, *70* (8), 2111−2124.

https://doi.org/10.1021/acs.cgd.2c01411
Cryst. Growth Des. 2023, 23, 1323−1329